Preprints (www.preprints.org) | NOT PEER-REVIEWED | Posted: 13 July 2018 doi:10.20944/preprints201807.0234.v1

Article

Novel Plasmonic Modes of Monolayer MoS_2 in the Presence of Spin-Orbit Interactions

Z.H. Tao[1], H.M. Dong [1,†], Y.F. Duan[1], F. Huang [2]

[1] School of Physical Science and Technology, China University of Ming and Technology, Xuzhou 221116, P. R. China

[2] Low Carbon Energy Institute, China University of Mining and Technology, Xuzhou 221116, P. R. China

* Correspondence: hmdong@cumt.edu.cn; Tel:+86-051683591580

Academic Editor: name

Version July 13, 2018 submitted to

Abstract: We investigate on the plasmons of monolayer MoS_2 in the presence of spin-orbit interactions (SOIs) under the random phase approximation. The theoretical study shows that two new and novel plasmonic modes can be achieved via inter spin sub-band transitions around the Fermi level duo to the SOIs. The plasmon modes are optic-like, which are very different from the plasmon modes reported recently in monolayer MoS_2, and the other two-dimensional systems. The frequency of such plasmons increases with the increasing of the electron density or the spin polarizability, and decreases with the increasing of the wave vectors q. Our results exhibit some interesting features which can be utilized to the plasmonic and terahertz devices based on monolayer MoS_2.

Keywords: plasmonic; spin-orbital couplings; plasmon

1. Introduction

It has been found that monolayer MoS_2 can be easily prepared by solvent [1] or pyrolysis [2]. Bulk material MoS_2 is an indirect band gap semiconductor, while monolayer MoS_2 is a direct band gap semiconductor, which can be widely applied to optoelectronic devices, such as electron probe, transistor manufacturing, etc. In 2011, Kis reported a switching ratio of 10^8 for MoS_2 field effect transistor (FET) [3], which indicates that monolayer MoS_2 can be made for the next generation of nano-electronic devices. Furthermore, it has been found that monolayer MoS_2 can be realized a strong light emission efficiency, which is 10^4 times that of ordinary bulk materials [4]. Recently, the plasmons and surface plasmons of monolayer MoS_2 have been widely investigated experimentally. Yong etc. proposed a graphene-MoS_2 hybrid nanostructure biosensor with enhanced surface plasmon resonance [5]. Lin and others found that photocurrent of MoS_2 transistor device can be increased significantly by the plasmonic resonant [6]. Surface plasmon resonances in graphene-MoS_2 hybrid structures enhance fiber optic sensors [7]. The tunable strong exciton-plasmon couplings in monolayer MoS_2 are observed in monolayer MoS_2 due to the involvings the resonances of excitons, plasmonic lattice, and localized surface plasmon [8]. It has been shown that plasmon induce energy transfer and photoluminescence manipulation in MoS_2 [9]. The large-area plasmon enhanced can be achieved in MoS_2 [10]. These important experimental findings shed further light on the applications of plasmonic nano-devices based on MoS_2.

However, the corresponding theoretical study lags rather behind the experimental activities on plasmons in MoS_2. Scholz etc. have investigated on the plasmons induced by the intra-spin subband transitions in monolayer MoS_2, considering the SOIs [11]. Furthermore, the energy bands of monolayer MoS_2 split off due to the SOIs, the new plasmon transitions between the different spin subbands can be achieved. In order to study the many body effect and plasmon within the SOIs in monolayer MoS_2 electronic systems and to develop plasmonic devices, we intend to study the novel plasmon modes of monolayer MoS_2 in the presence of SOIs, and find some interesting features of such novel plasmons.

2. Theoretical approach

The bulk material MoS_2, a rhombohedral crystal or hexagonal crystal structure, is formed by stacking individual monolayer. Each monolayer is a sandwich-like structure of two layers of S atoms stacked with a layer of Mo atoms. Each Mo atom is surrounded by six S atoms within the layer, which are covalently bonded to form a triangular prism-shaped coordination structure. Six S atoms are distributed at each tip of the triangular prism. Each Mo atom combines with four S atoms, and each S atom combines with three Mo atoms. The bond length of Mo-S is 0.24 nm, and the bond length of S-S is 0.32 nm. The S-Mo-S bond angle is 80.68° [12]. The MoS_2 layers are interconnected by weak Van der Waals force. One can obtain monolayer MoS_2 by cutting off the force between connected layers from bulk material MoS_2.

In the low energy region, we can describe electronic movement near K-point by the following effective Hamiltonian [13]

$$H(\mathbf{k}) = \begin{bmatrix} \Delta/2 & at(k_x - ik_y) \\ at(k_x + ik_y) & -\Delta/2 + s\gamma \end{bmatrix}, \tag{1}$$

where the lattice parameter $a = 3.19$, the nearest hoping parameter $t = 1.1$ eV. $\mathbf{k} = (k_x, k_y)$ is wave-vector for a carrier. $s = \pm 1$ respectively index spin up and down. $\gamma = 75$ meV is strength of spin-orbit coupling and the band gap energy $\Delta = 1.66$ eV [14]. Solving the Schrödinger equation, the energy spectrum of monolayer MoS_2 are readily obtained, which read

$$E^s_\lambda(\mathbf{k}) = s\gamma/2 + \lambda\sqrt{\varsigma^2 k^2 + (\Delta - s\gamma)^2/4}, \tag{2}$$

Here $\lambda = \pm 1$ refers to the conduction bands and the valence bands in monolayer MoS_2, $\varsigma = at$ and $k = (k_x^2 + k_y^2)^{1/2}$. Moreover, the corresponding wave functions are obtained as

$$\psi^s_{\lambda,\mathbf{k}}(\mathbf{r}) = N^s_\lambda(\mathbf{k})[\varsigma k e^{-i\phi}/B^s_\lambda(\mathbf{k}), 1]e^{\mathbf{k}\cdot\mathbf{r}}, \tag{3}$$

with $\mathbf{r} = (x, y)$, $B^s_\lambda(\mathbf{k}) = E^s_\lambda(\mathbf{k}) - \Delta/2$, $N^s_\lambda(\mathbf{k}) = |B^s_\lambda(\mathbf{k})|/[(B^s_\lambda(\mathbf{k}))^2 + \varsigma^2 k^2]^{1/2}$, ϕ is the angle between $\mathbf{k}$ and x axis.

The energy spectrum with the spin splittings are shown in Fig. 1. It shows the conduction band splits into two spin subbands. For a fixed Fermi energy E_F, the Fermi wavevector $k_F^{\pm}$ in different spin sub-bands are obtained as

$$k_F^{\pm} = \frac{1}{\varsigma}\sqrt{(E_F \mp \gamma/2)^2 - (\Delta \mp \gamma)^2/4}, \tag{4}$$

which indicates that the electrons in different sub-bands are able to change their spin orientation simply through momentum exchange via inter-spin transition channels [15].

We now consider the electron-electron (e-e) interactions in different spin sub-bands in the conduction bands ($\lambda = +1$), the effective e-e interactions in monolayer MoS_2 is

$$V_e(\mathbf{q}, \omega) = \varepsilon_{s's}(\mathbf{q}, \omega)V(\mathbf{q}, \omega), \tag{5}$$

where $V(\mathbf{q}, \omega)$ is the bare e-e interactions in monolayer MoS_2. Under the random-phase approximation (RPA), the dielectric function can be written as

$$\varepsilon_{s's}(\mathbf{q}, \omega) = V_e(\mathbf{q}, \omega)/V(\mathbf{q}, \omega) = 1 - V(\mathbf{q})\Pi_{s's}(\mathbf{q}, \omega). \tag{6}$$

Here $\Pi_{s's}(\mathbf{q}, \omega)$ is the density-density correlation, which reads

$$\Pi_{s's}(\mathbf{q}, \omega) = \sum_{\mathbf{k}} \frac{f_{s'}(\mathbf{k}+\mathbf{q}) - f_s(\mathbf{k})}{E_{s'}(\mathbf{k}+\mathbf{q}) - E_s(\mathbf{k}) + \hbar\omega_{s's} + i\eta}. \tag{7}$$

Preprints (www.preprints.org) | NOT PEER-REVIEWED | Posted: 13 July 2018 doi:10.20944/preprints201807.0234.v1

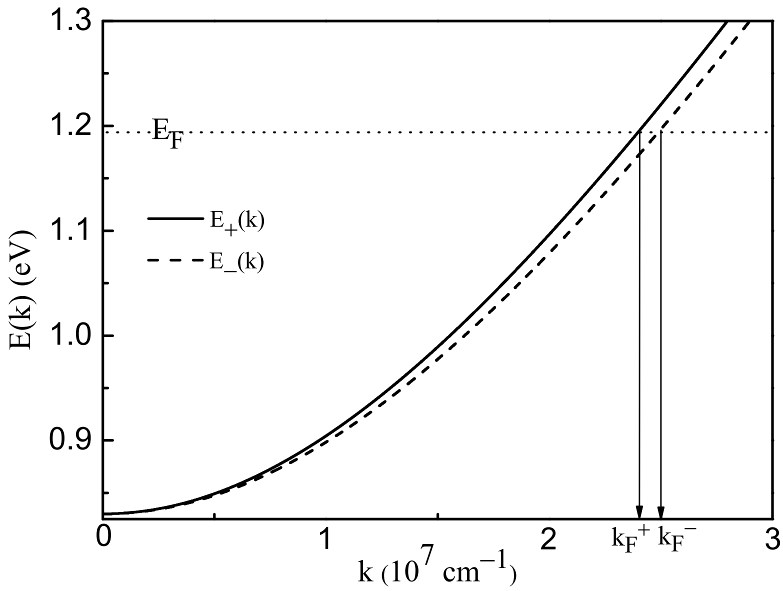

Figure 1. Energy function E (k) versus k for the monolayer MoS_2 in different spin branches. E_F (broken curve) is the Fermi energy and the intersections of the curves for $E_\pm(k)$ with the Fermi level, projected onto the k axis, give the Fermi wavevectors k_F^- and k_F^+.

$\omega_{s's}$ is the scattering frequency induced by inter spin-subband transitions ($s' \neq s$), $\eta \to 0$, $\mathbf{q} = (q_x, q_y)$ is the change of the wave vector, $v_q = 2\pi e^2/\kappa q$ is the two-dimensional Fourier transform of the e-e Coulomb interactions with κ being the high frequency dielectric constant, $f(x)$ is Fermi-Dirac distribution function.

The plasmon modes can be determined by the real part of the dielectric function $\mathrm{Re}[\varepsilon(\mathbf{q}, \omega)] = 0$. Due to the Landau damping, the plasmon of the electronic systems can decay into the single particle excitations, such as electron-hole pairs, which leads to the instability of the element excitations. In general, when the wave vector $\mathbf{q}$ of the element is large, the elementary excitation will degenerate into the excitations of the electron-hole pairs. The damped elementary excitation cannot be observed experimentally. In order to study the many body interactions among electrons, we consider the case of temperature $T \to 0$. Considering $\gamma \ll \Delta$, we obtain the undamped plasmon modes between the different spin subbands in the conduction bands, which are

$$\omega_{+-} = \omega_0(\frac{q_{+-}}{q} - 1), \tag{8}$$

induced by the inter-spin subband transitions from the spin down subband ($s = -$) to the spin up subband ($s' = +$), and

$$\omega_{-+} = \omega_0(\frac{q_{-+}}{q} + 1) \tag{9}$$

induced by the inter-spin subband transitions from the spin up subband ($s = +$) to the spin down subband ($s' = -$). $\omega_0 = \gamma/\hbar \simeq 17.86$ THz, $q_{+-} = 2\pi e^2 \alpha_{+-} n_e/(\hbar\kappa\omega_0)$ with $\alpha_{+-} = (n_+ - n_-)/n_e$ and $q_{-+} = 2\pi e^2 \alpha_{-+} n_e/(\hbar\kappa\omega_0)$ with $\alpha_{-+} = (n_- - n_+)/n_e$, $\kappa = 5$ for monolayer MoS_2 [11].

3. Results and discussions

In figure 2, the dispersions of the plasmon frequencies ω_{+-} are shown for the different electron densities n_e (upper panel) and the different spin polarizabilities α_{+-} (lower panel). The plasmons with the frequencies ω_{+-} are induced by the inter-spin subband transitions of electrons from the spin down subband ($-$) to the spin up subband ($+$) in monolayer MoS_2. The upper panel shows that the plasmon frequency ω_{+-} heavily depends on the plasmon wave vector q and the electron densities n_e.

 doi:10.20944/preprints201807.0234.v1

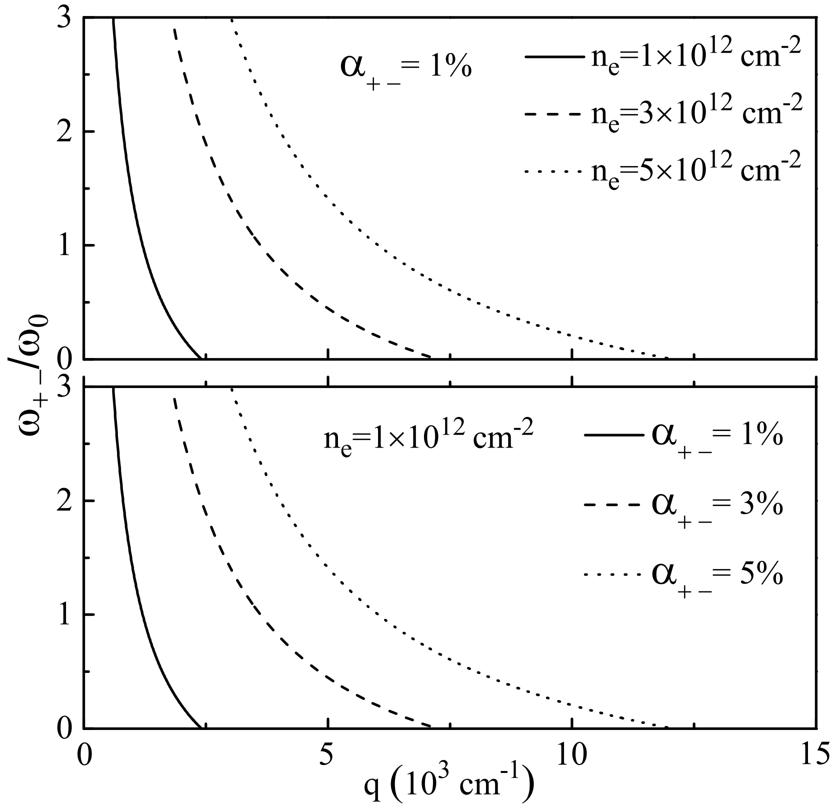

Figure 2. Dispersion relations of the plasmon frequencies ω_{+-} induced by the inter-spin subband transitions of electrons from the spin down subband $(-)$ to the spin up subband $(+)$ in monolayer MoS_2 for the different electron densities n_e (upper panel) and the different spin polarizabilities α_{+-} (lower panel).

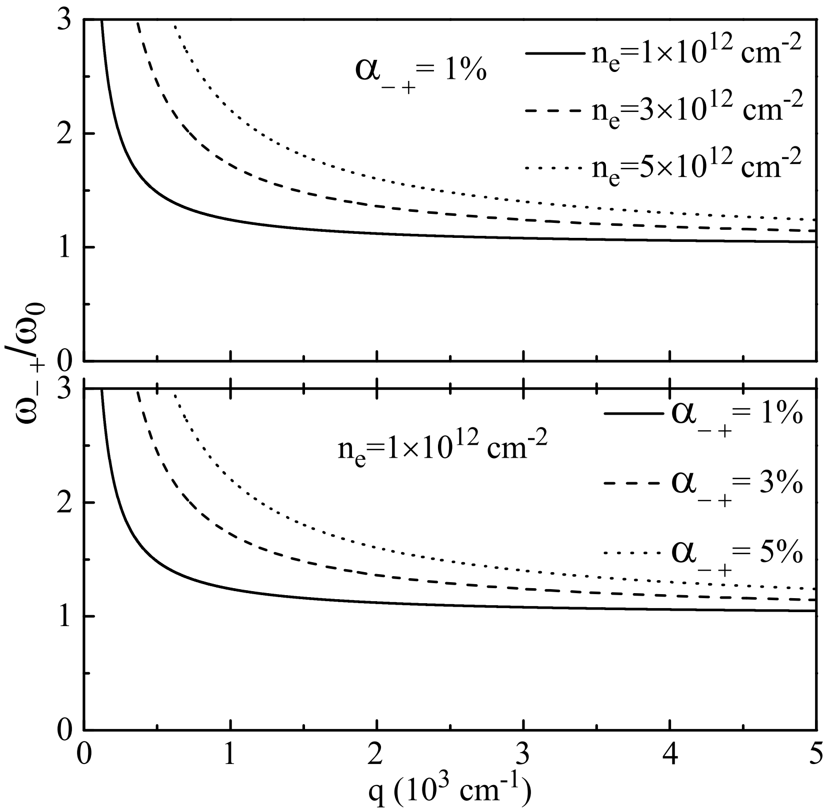

Figure 3. Dispersion relations of the plasmon frequencies ω_{-+} induced by the inter-spin subband transitions of electrons from the spin down subband ($-$) to the spin up subband ($+$) in monolayer MoS_2 for the different electron densities n_e (upper panel) and the different spin polarizabilities α_{-+} (lower panel).

the plasmon frequency ω_{+-} rises as the electron density n_e increases, but decreases with the increasing q. In addition, the lower panel shows that the plasmon frequency ω_{+-} strongly depends on the spin polarizabilities α_{+-}, and ω_{+-} are enlarged when the spin polarizability α_{+-} increases at the same q and n_e. Actually, ω_{+-} is proportional to q^{-1} (see equation 8), which is essentially optic-like plasmon modes. Moreover, the plasmon frequency ω_{+-} reduce to 0 as q rise to q_{+-}, which can be obtained from equation 8. As shown in figure 2, the larger the n_e or α_{+-} is, the more gradually the dispersion curves decrease for the same ω_{+-}. This indicates that we obtain a wider q range that can be used to control the frequency ω_{+-}. This interesting feature of ω_{+-} means that the plasmon frequency ω_{+-} can be easily modulated with the high n_e or α_{+-}. Importantly, we have found that ω_{+-} can be located in terahertz frequency.

Figure 3 shows the dispersions of the plasmon frequencies ω_{-+} for the different electron densities n_e (upper panel) and the different spin polarizabilities α_{-+} (lower panel). The plasmons ω_{-+} are induced by the inter-spin subband transitions of electrons from the spin up subband ($+$) to the spin down subband ($-$) in monolayer MoS_2. In the small q value region, the plasmon frequency ω_{-+} strongly depends on the wave vector q, the electron density n_e (see upper panel) and the polarizability α_{-+} (seen lower panel). The frequency ω_{-+} is increased as n_e or α_{-+} enlarging but decrease with the increasing q in the small q region. In the large q region, ω_{-+} depends frailly on n_e, α_{-+} and q, which is finally close to ω_0. It shows that the plasmon modes of ω_{-+} can be applied to measure the strength γ of the SOIs experimentally because of $\omega_0 = \gamma/\hbar$. Moreover, for the greater n_e or α_{-+}, ω_{-+} tend to ω_0 more slowly. From equation 9, ω_{-+} is proportional to q^{-1} and the plasmon modes are actually optic-like. In fact, ω_{-+} can also be located in the terahertz band, which is similar to ω_{+-}.

The frequencies ω_{-+} and ω_{+-} of the both plasmons induced by inter-spin subband transitions in monolayer MoS_2 are both strongly depend on q, n_e and spin polarizabilities α, which can be modulated. With the suitable q, α and n_h value, the two novel plasmon modes can also be located in terahertz range, which shows a potential application of the monolayer MoS_2 in terahertz devices. In addition, ω_{+-} and ω_{-+} are generally proportional to q^{-1}, the two novel plasmon modes are essentially optic-like in our work. However, the plasmon frequencies induced by the intra-subband transitions in monolayer MoS_2 and the two-dimensional electron gas system are proportional to $q^{1/2}$ [13,15], which are acoustic-like. Normally, we can measure optical-like plasmon modes by optical experiments, such as optical absorption spectroscopy, Raman spectrum, ultrafast pump-and-probe experiments, etc, while acoustic-like plasmon modes are not easy to be measured [17]. Consequently, we can examine the novel plasmonic devices based on the two new plasmons in monolayer MoS_2 by optical experiments. Furthermore, since these two novel plasmons are optical-like modes, we can achieve very high-frequency plasmons, which sheds light on the developments of high-frequency plasmon devices.

4. Conclusion

The novel and new optic-like plasmon modes induced by the inter spin subband transitions are achieved in monolayer MoS_2 due to the SOIs. The both frequencies of the plasmon frequencies distinctly decrease as the wave vector increases. By increasing of the electron density or the spin polarizability, the plasmon frequencies increase significantly. This paper points out that the two novel plasmon modes strongly depend on the electron density, the spin polarizability and the wave vector of incident light. We have obtained the two novel terahertz plasmon modes. Moreover, the two obtained plasmon modes are very different from those reported in monolayer MoS_2 and the two-dimensional electron gas systems. These results could be relevant for the potential applications of monolayer MoS_2 in advanced plasmonic and terahertz devices.

Acknowledgments: This work was supported by the National Natural Science Foundation of China (Grant Nos. 11604380, 11604192, and 61372048), and the Provincial Natural Science Foundation of Jiangsu (Grant No. BK20151138).

References

1. Novoselov K.S., Jiang D., Schedin F., Booth T.J., Khotkevich V.V., Morozov S.V., and Geim A.K., *Proc. Natl. Acad. Sci.*, **30** (2005) 10451.
2. Coleman J.N., Lotya M., OiNeil A., Bergin S.D., King P.J., et al., *Science*, **331** (2011) 568.
3. Radisavljevic B., Radenovic A., Brivio J., Giacometti V., and Kis A., *Nat. Nanotechnol.*, **6** (2010) 147.
4. Mak K.F., Lee C., Hone J., Shan J., and Heinz T.F., *Phys. Rev. Lett.*, **105** (2010) 136805.
5. Zeng S., Hu S., Xia J., Anderson T., Dinh X.Q., Meng X.M., Coquet P., Yong K.T., *Sens. Act. B*, **207** (2014) 801.
6. Lin J., Li H., Zhang H., and Chen W., *Appl. Phys. Lett.*, **102**, (2013) 203109.
7. Wei W., Nong J.P., Tang L.L., Wang N., Chuang C.J., Huang Y., *Plasmonic*, **12** (2017) 1205.
8. Liu W.J., Lee B.S., Naylor C.H., Ee H.S., Park J., Charlie Johnson A.T., and Agarwal R., *Nano Letts.* **16** (2016) 1262.
9. Yan J.H, Ma C.R., Liu P., and Yang G.W., *ACS Photonics*, **4** (2017) 1092.
10. Lee M.G., Yoo S.J., Kim T.H. and Park Q.H., *Nanoscale*, **9** (2017) 16244.
11. Scholz A., Stauber T., and Schliemann J., *Phys. Rev. B*, **88** (2013) 035135.
12. Scalise E., Houssa M., Pourtois G., Afanasev V., Stesmans A., *Nano Res.*, **5** (2012) 43.
13. Xiao D., Liu G.B., Feng W., Xu X., and Yao W., *Phys. Rev. Lett.*, **108** (2012) 196802.
14. Li Z., Carbotte J.P., *Phys. Rev. B*, **86** (2012) 205425.
15. Xu W., and Lin L.B., *J. Phys. Condens. Matter*, **16** (2004) 1777.
16. Tao Z.H., Dong H.M., *Acta Phys. Sin.* **66** (2017) 247701.
17. Vo*β*eb*ü*rger M., Roskos H.G., Wolter F., Waschke C. and Kurz H., *J. Opt. Soc. Am. B*, **13** (1996) 1045.